Squeezing Quantum Many-Body Scars

Bennet Windt[1,2,3] and Hannes Pichler[1,4,*]

[1]Institute for Quantum Optics and Quantum Information, Austrian Academy of Sciences, 6020 Innsbruck, Austria
[2]Blackett Laboratory, Imperial College London, Prince Consort Road, London SW7 2AZ, United Kingdom
[3]Max Planck Institute of Quantum Optics, Hans-Kopfermann-Straße 1, 85748 Garching, Germany
[4]Institute for Theoretical Physics, University of Innsbruck, 6020 Innsbruck, Austria

(Received 10 June 2021; accepted 27 January 2022; published 4 March 2022)

We develop an analytical approach for the description of quantum many-body scars in PXP models. We show that the scarred dynamics in the PXP model on a complete bipartite graph can be interpreted as a one-dimensional chiral scattering problem, and solve this problem analytically. The insights from this analysis allow us to predict that dynamical signatures of scars in PXP models can be enhanced by spin squeezing the initial states. We show numerically that this stabilization mechanism applies not only to the complete bipartite graph but also to one- and two-dimensional lattices, which are relevant for Rydberg atom array experiments. Moreover, our findings provide a physical motivation for Hamiltonian deformations reminiscent of those known to produce perfect scars.

DOI: 10.1103/PhysRevLett.128.090606

When a quantum many-body system is brought out of equilibrium, its constituents typically relax to their individual equilibrium states, in a process referred to as thermalization [1,2]. Importantly, thermalization occurs even in closed quantum systems, since the different constituents of an interacting many-body system can act as a reservoir for each other. This paradigm provides a very powerful framework for understanding the emergence of statistical mechanics from a microscopic perspective [3].

Recently, quantum many-body scarring, a novel phenomenon that defies this paradigm, has gained significant interest [4]. Quantum many-body scars (QMBS) have been discovered in quantum simulation experiments with Rydberg atom arrays [5], where certain ordered initial states undergo periodic dynamics, in contrast to the expected relaxation of local observables to stationary, thermal values. Since then, significant research efforts have been devoted to uncovering mechanisms which underlie and enhance this phenomenon [6–9]. While scars have since been discovered also in other models [10–19], their origin in the original Rydberg model remains not completely understood. Various methods to address this problem have been employed, including Krylov subspace methods [20,21] and variational approaches [22,23].

In this work, we introduce a complementary approach, by mapping the dynamics associated with QMBS in Rydberg atom arrays onto a scattering problem in an appropriate limiting case. We provide an analytical solution of this scattering problem, whose interpretation offers a new perspective on the mechanisms underlying QMBS. As an immediate application we also identify physical mechanisms by which the dynamical signatures of scars can be enhanced. Specifically, the scattering matrix suggests an enhancement of the periodic revivals by squeezing the initial states, which we confirm numerically for various lattices. Moreover, our approach also provides a clear physical motivation for Hamiltonian deformations to PXP models that result in perfect QMBS, which have been introduced *ad hoc* in previous studies [6,7].

Model.—To understand the dynamics of scars in Rydberg atom arrays, we work within the well-established PXP approximation [24]. Specifically, we consider a graph $G = (V, E)$ with vertices V and edges E, which induces a PXP model as follows: we identify each vertex $i \in V$ with a qubit with states $|0\rangle_i$ and $|1\rangle_i$, and introduce a projection operator P_e for each edge $e = \{i, j\} \in E$ as $P_e = \mathbb{1} - |1\rangle_i\langle 1| \otimes |1\rangle_j\langle 1|$. We call the common eigenspace of all these commuting projectors with eigenvalue $+1$ the constrained space $\mathcal{H}_P$. It contains all states with no neighboring qubits simultaneously in state $|1\rangle$, akin to a nearest-neighbor approximation of the Rydberg-blockade constraint [25–27]. The projector onto this space is denoted $\mathcal{P} = \prod_{e\in E} P_e$. Within $\mathcal{H}_P$, dynamics are governed by the so-called PXP Hamiltonian,

$$H = \frac{\Omega}{2}\sum_{i=1}^{N} \mathcal{P}\sigma_i^x\mathcal{P}, \tag{1}$$

which has a simple interpretation: each qubit undergoes single particle Rabi oscillations if all its neighbors are in the state $|0\rangle$, while its dynamics are frozen if at least one of its neighbors is in the state $|1\rangle$. Despite its simple form, the conditional dynamics render the Hamiltonian generically nonintegrable [4].

We are interested in PXP models on bipartite graphs, $V = A \cup B$, where A and B denote the two partitions. On such graphs, $\mathcal{H}_P$ contains two extremal states $|\mathbb{Z}_2^A\rangle$ and $|\mathbb{Z}_2^B\rangle$, where all qubits $i \in A$ are in the state $|1\rangle_i$ and all qubits $i \in B$ are in state $|0\rangle_i$ for $|\mathbb{Z}_2^A\rangle = |1\rangle^{\otimes i\in A}|0\rangle^{\otimes i\in B}$ and vice versa for $|\mathbb{Z}_2^B\rangle = |0\rangle^{\otimes i\in A}|1\rangle^{\otimes i\in B}$. These states play an important role for scars in PXP models; specifically, it was discovered in Ref. [5] that in one dimension (1D), these states undergo approximate periodic dynamics, with alternating revivals of the two $\mathbb{Z}_2$ states: $e^{-iHT_{1D}/2}|\mathbb{Z}_2^A\rangle \approx |\mathbb{Z}_2^B\rangle$ and $e^{-iHT_{1D}/2}|\mathbb{Z}_2^B\rangle \approx |\mathbb{Z}_2^A\rangle$, with $T_{1D} \approx 2\pi \times 1.51\ \Omega^{-1}$. Recently, experiments with Rydberg atom arrays observed analogous scars in bipartite lattices in two dimensions (2D) [8]. Importantly, such periodic dynamics imply that the $\mathbb{Z}_2$ states have non-negligible overlap with only an extensive number of equally spaced, atypical eigenstates of the Hamiltonian, the so-called quantum many-body scars [20].

To develop an intuitive interpretation of these periodic dynamics, we find it convenient to first consider a special limiting case: the complete bipartite graph (CBG), where each site in A is neighboring to each site in B, i.e., $E = \{\{i, j\}|i \in A, j \in B\}$, with $|A| = |B| = N/2$, resulting in $\dim(\mathcal{H}_P) = 2^{N/2+1} - 1$ (see Fig. 1). In the thermodynamic limit $N \to \infty$, we will show below that the scar dynamics on this graph map onto a 1D scattering problem that can be solved analytically.

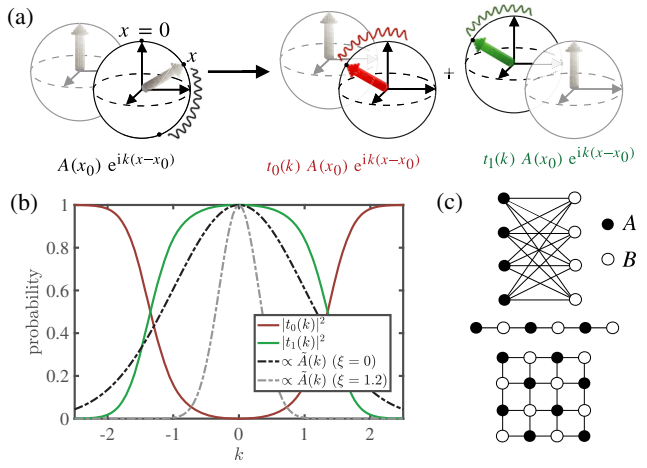

FIG. 1. (a) Schematic illustration of the scattering problem. States on either bipartition of a CBG are represented on a generalized Bloch sphere, parametrized by a position observable x along a great circle. An incident plane wave (wave number k) on partition A, with partition B in the vacuum state (left), is scattered into a superposition with one of the two partitions in the vacuum state (right). (b) Scattering probabilities $|t_0(k)|^2$ and $|t_1(k)|^2$ and unsqueezed ($\xi = 0$) and squeezed ($\xi = 1.2$) wave functions of the $\mathbb{Z}_2$ state. (c) While the scattering picture applies to the CBG (top), key insights generalize to other bipartite lattices, such as the 1D line or 2D square lattice.

On the CBG, the PXP Hamiltonian simplifies to

$$H = \hat{S}_A^x \otimes |\phi\rangle_B\langle\phi| + |\phi\rangle_A\langle\phi| \otimes \hat{S}_B^x, \tag{2}$$

where we have set $\Omega = 1$ for simplicity and defined global spin operators in bipartiton A as $\hat{S}_A^\mu = 1/2\sum_{i\in A}\sigma_i^\mu$ ($\mu \in \{x, y, z\}$) and analogously for B. The states $|\phi\rangle_A = |0\rangle^{\otimes i\in A}$ and $|\phi\rangle_B = |0\rangle^{\otimes i\in B}$ denote the state where all qubits $i \in A$ or $i \in B$ are in the $|0\rangle_i$ state, respectively. We refer to $|\phi\rangle$ as the vacuum state. Whenever it is clear from the context we drop the subscripts indicating the partition. For the CBG, a general time-dependent state may be written as

$$|\psi(t)\rangle = |A(t)\rangle \otimes |\phi\rangle + |\phi\rangle \otimes |B(t)\rangle. \tag{3}$$

Note that $|\psi(t)\rangle$ is normalized but $|A(t)\rangle$ and $|B(t)\rangle$ are not individually normalized. This form highlights explicitly the fact that partition A can only be in a state other than the vacuum state if partition B is in the vacuum state, and vice versa. The time-dependent Schrödinger equation for a state (3) associated with the Hamiltonian (2) takes the form of two coupled equations:

$$\begin{aligned} i\partial_t|A(t)\rangle &= \hat{S}^x|A(t)\rangle + \langle\phi|B(t)\rangle\hat{S}^x|\phi\rangle, \\ i\partial_t|B(t)\rangle &= \hat{S}^x|B(t)\rangle + \langle\phi|A(t)\rangle\hat{S}^x|\phi\rangle. \end{aligned} \tag{4}$$

Evidently, the coupling is governed by the overlap of the state on either partition with the vacuum state. For a random state, this overlap is exponentially small in the system size N and can be neglected. In this approximation, the decoupled equations can be trivially solved: the solution is simply a global rotation of all spins in the active partition, i.e., $|A(t)\rangle = e^{-i\hat{S}^x t}|A(0)\rangle$ and $|B(t)\rangle = e^{-i\hat{S}^x t}|B(0)\rangle$, respectively. Importantly, one can check for each approximate solution that the overlap with the vacuum state remains exponentially small at all times, thus justifying the decoupling approximation *a posteriori*. Crucially, for the $\mathbb{Z}_2$ initial states the decoupling approximation breaks down after some finite time. This allows us to distinguish two types of dynamics induced by (2): trivial oscillatory dynamics of uncoupled partitions, and dynamics of coupled partitions. Even though the former is largely irrelevant for our analysis, it is important to stress that it is associated with an approximate integrability of each partition. This is a peculiarity of the CBG: on other bipartite graphs, the PXP Hamiltonian is chaotic and thermalizing for generic initial states [20]. This approximate integrability on the CBG can be easily removed without affecting the dynamics of the $\mathbb{Z}_2$ states, for example, by including additional integrability-breaking terms in the Hamiltonian that vanish on all states that are invariant under permutations of spins within a partition. An explicit example of such a construction is given in Ref. [7]. We stress that our

analysis of the dynamics of the $\mathbb{Z}_2$ states on the CBG thus holds also in such chaotic versions of the CBG.

Scattering problem.—For the remainder of this work, we focus on the nontrivial dynamics resulting from the $\mathbb{Z}_2$ initial states. For the sake of concreteness, we choose A as the initially active partition, i.e., $|A(0)\rangle = |S, \theta_0 = \pi, \varphi_0 = \pi/2\rangle$ and $|B(0)\rangle = 0$, where we have defined spin coherent states $|S, \theta, \varphi\rangle \equiv [\cos(\theta/2)|0\rangle + e^{-i\varphi}\sin(\theta/2)|1\rangle]^{\otimes N/2}$ [28]. Neglecting any coupling between the partitions, these states evolves as $|A(t)\rangle = |S, \pi - t, \pi/2\rangle$ and $|B(t)\rangle = 0$. The overlap of the spin coherent state $|S, \theta, \pi/2\rangle$ with the vacuum state is given by $\langle\phi|S, \theta, \pi/2\rangle = \cos^{N/2}(\theta/2) \overset{N\gg 1}{\to} \exp(-N\theta^2/8)$ [35]. This justifies the decoupling approximation for times $t \lesssim \pi - 2/\sqrt{N}$. At later times, however, the state then enters a narrow neighborhood of the vacuum state and the coupling between the two partitions needs to be taken into account properly. A suitable framework to tackle the dynamics in this regime is the Holstein-Primakoff transformation [28], which embeds the Hilbert space containing states close to the vacuum state in that of a bosonic mode via

$$\hat{x} = \frac{i}{\sqrt{2}}(\hat{a}^\dagger - \hat{a}) = -\frac{1}{\sqrt{S}}\lim_{S\to\infty}\hat{S}^y,$$
$$\hat{p} = \frac{1}{\sqrt{2}}(\hat{a}^\dagger + \hat{a}) = \frac{1}{\sqrt{S}}\lim_{S\to\infty}\hat{S}^x, \tag{5}$$

where $\hat{a}$ is the bosonic ladder operator that annihilates the vacuum $|0\rangle = \lim_{N\to\infty}|\phi\rangle$, and where $S = N/4$. The eigenstates of $\hat{x}$ and $\hat{p}$ with eigenvalues x and p are denoted by $|x\rangle$ and $|p\rangle$, respectively. Here, x is identified with the (rescaled) position on the $\varphi = \pi/2$ great circle of the spin coherent state Bloch sphere, $x \sim \sqrt{S}\theta$.

We proceed in solving the coupled equations (4) in the vicinity of the vacuum state by constructing the eigenstates of the associated time-independent Schödinger equation in the position basis. That is, we consider solutions of the form $|A(t)\rangle = e^{-iEt}|A\rangle$ and $|B(t)\rangle = e^{-iEt}|B\rangle$, where the eigenstates in the position basis, $A(x) = \langle x|A\rangle$ and $B(x) = \langle x|B\rangle$, satisfy

$$A'(x) = ikA(x) - \langle\phi|B\rangle\phi'(x),$$
$$B'(x) = ikB(x) - \langle\phi|A\rangle\phi'(x). \tag{6}$$

Here, we have introduced the rescaled energy eigenvalue $k = E/\sqrt{S}$ and we use the notation $f'(x)$ to indicate the derivative of $f(x)$ with respect to x. The vacuum state in this position basis is $\phi(x) = \pi^{-1/4}e^{-x^2/2}$ (see Supplemental Material [28]).

The coupled differential equations (6) can be interpreted as a scattering problem for two chiral channels coupled by a short range nonlocal potential. In both channels, A and B, the system can freely propagate toward increasing x, except in the vicinity of $x = 0$, where the channels are coupled. There the system can either remain in the same channel or scatter into the other channel, before leaving the scattering region. The relevant data characterizing the scattering solutions are thus the (energy dependent) transmission coefficients $t_0(k)$ and $t_1(k)$, associated with no change of the channel and a flip of the channel in the scattering process, respectively (see Fig. 1). The chiral nature and the elasticity of the scattering process guarantee $|t_0(k)|^2 + |t_1(k)|^2 = 1$.

We can formally solve the differential equations (6) to obtain analytical expressions for both scattering coefficients $t_0(k)$ and $t_1(k)$, conveniently expressed using the short-hand notation for the (iterated) Gaussian integrals $G(k) = \int_{-\infty}^{\infty}\phi(z)e^{ikz}dz$, $H(k,x) = \int_{x_0}^{x}\phi'(z)e^{-ikz}dz$, and $F(k) = \int_{-\infty}^{\infty}\phi(z)e^{ikz}H(k,z)dz$. The solutions read $t_0(k) = 1 + G(k)F(k)H(k)/[1 - F(k)^2]$ and $t_1(k) = G(k)H(k)/[F(k)^2 - 1]$, with $H(k) = \lim_{x\to\infty}H(k,x)$ [28]. The transmission coefficients are system size independent and the associated probabilities $|t_0(k)|^2$ and $|t_1(k)|^2$ are shown in Fig. 1. Importantly, $t_0(0)$ vanishes exactly, corresponding to perfect transfer between the channels at zero energy, i.e., $|t_1(0)| = 1$. This leads to a transfer window of width ~ 1 around $k = 0$. The scattering phase shift at zero energy, $\zeta_1 = i(1/t_1)(dt_1/dk)|_{k=0}$, evaluates numerically to $\zeta_1 = 2.014$. In the opposite limit of $|k| \gg 1$, the two channels effectively decouple.

The initial state of interest here, $|\mathbb{Z}_2^A\rangle$, corresponds to an incoming Gaussian wave packet in channel A, i.e., $\langle x|A(t=0)\rangle = \pi^{-1/4}e^{-(x-S\pi)^2/2}$ and $\langle x|B(t=0)\rangle = 0$. Its decomposition into scattering eigenstates is thus also Gaussian, with Fourier amplitudes $\tilde{A}(k) = 2^{1/2}\pi^{1/4}e^{-k^2/2}$. The probability $P_1 = (1/2\pi)\int_{-\infty}^{\infty}|t_1(k)\tilde{A}(k)|^2dk$ of a change of channel at the first scattering event evaluates to $P_1 \approx 0.906$. After the scattering event, one can again apply the decoupling approximation, to propagate the wave function between subsequent scattering events at $t \approx (2\mathbb{N} + 1)\pi$, showing that a large value for P_1 is required for the expected alternating (approximate) revivals of the two $\mathbb{Z}_2$ states. The quality of these revivals is quantified by the many-body fidelity $g(t) = |\langle\psi(0)|\psi(t)\rangle|$, which is displayed in Fig. 2. It shows alternating smaller and larger peaks, where the former (at $\Omega t \approx 2\pi$) result from the finite probability of the system not changing channel in the scattering process ($1 - P_1 \approx 0.094$), while the latter (at $\Omega t \approx 4\pi$) appears due to two consecutive scattering processes resulting in two successive changes of channel. The height of this first (large) revival of $g(t)$, which we denote $g_{\max}$, can thus be calculated as

$$g_{\max} = \left|\frac{1}{2\pi}\int_{-\infty}^{\infty}e^{i\tau}\tilde{A}_2(k)\tilde{A}(k)^*dk\right|, \tag{7}$$

where $\tilde{A}_2(k) = (t_0(k)^2 + t_1(k)^2)\tilde{A}(k)$ is the wave function of the state on bipartition A after two scattering events

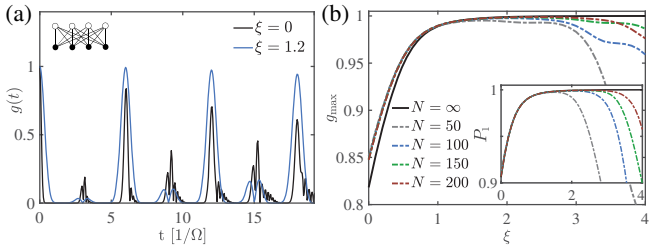

FIG. 2. (a) Many-body fidelity $g(t)$ for a CBG with $N = 200$, initialized in both an unsqueezed ($\xi = 0$) and a squeezed ($\xi = 1.2$) initial $\mathbb{Z}_2$ state. (b) Maximal revival fidelity $g_{\max}$, and transmission probability P_1 (inset) as a function of the squeezing parameter ξ for various system sizes. We note a finite-size effect at high squeezing, which occurs when squeezing expands the spin coherent state around a great circle of a finite-radius Bloch sphere.

and the phase τ is introduced to account for the phase shift acquired by $\tilde{A}_2(k)$ relative to $\tilde{A}(k)$. Since $|t_1(k)^2\tilde{A}(k)| \gg |t_0(k)^2\tilde{A}(k)|$, as a first approximation we may choose $\tau = 2\zeta_1$ for which $g_{\max} \approx 0.818$. The exact phase shift maximizing $g_{\max}$ can be determined numerically as $\tau = 3.55$ and results in $g_{\max} \approx 0.846$. The fact that $g_{\max} < 1$ reflects the fact that the PXP models host only approximate QMBS.

Squeezed QMBS.—The scattering picture directly suggests the possibility of constructing different initial states which will display enhanced revivals. Specifically, the transfer window at $k = 0$ (see Fig. 1) indicates that P_1 and $g_{\max}$ could be increased by squeezing the width of the initial state momentum distribution $\tilde{A}(k)$ below 1. A natural candidate is the class of spin squeezed states [36–38], defined as $|S, \theta, \varphi; \chi\rangle = V_\chi |S, \theta, \varphi\rangle$ with

$$V_\chi = e^{\chi/2[(\hat{S}^+)^2 - (\hat{S}^-)^2]}. \tag{8}$$

A squeezed $\mathbb{Z}_2$ initial state $|\psi(0)\rangle = V_\chi \otimes \mathbb{1}|\mathbb{Z}_2^A\rangle$ thus corresponds to a squeezed Fourier wave packet $\tilde{A}(k) = 2^{1/2}\pi^{1/4}e^{-k^2e^{2\xi}/2+\xi/2}$, with $\xi = \chi N/2$. As shown in Fig. 2, squeezing the initial states indeed leads to larger and more long-lived revivals with increasing ξ [until finite system size effects become relevant at $\xi \sim \log(N)$].

Even though the scattering problem is rigorously defined only on the infinite CBG, we find that spin squeezing of the initial $\mathbb{Z}_2$ states leads to enhanced revivals in PXP models also on other bipartite graphs. This requires a generalization of the spin squeezing operator. A physically motivated choice that takes into account the locality on a given bipartite graph is the quasilocal transformation

$$U_\chi = e^{\chi/2\sum_{i\in B}[(\hat{S}_i^+)^2 - (\hat{S}_i^-)^2]}. \tag{9}$$

Here, the $\hat{S}_i^\pm$ denote the ladder operators for the compound spin systems of the nearest neighbors of the ith site. For instance, in the case of a circle of N sites,

$$\hat{S}_i^\pm = \frac{1}{2}\sigma_{i-1}^\pm + \frac{1}{2}\sigma_{i+1}^\pm, \tag{10}$$

where the addition in the subscript is modulo N. We will refer to this as local squeezing, while we dub the transformation (8) global squeezing. The physical reasoning underlying this choice of squeezing operator is the following. Each spin on partition B is initially blockaded by its z nearest neighbors and frozen in the state $|0\rangle_i$. From the perspective of this spin, this is analogous to the situation in a CBG of size $2z$. Based on our results for the CBG, we may expect that squeezing of the initial state of its nearest neighbors liberates that particular spin most efficiently, resulting in more pronounced revivals. Applying this argument to all spins in partition B implies (9).

We solve for the dynamics of squeezed initial states in the 1D chain and 2D square lattice (with periodic boundary conditions) by numerical integration of the corresponding Schrödinger equation on finite system sizes, and compare the local squeezing approach (9) with a naive application of a global squeezing operation (see Fig. 3). For small squeezing, both approaches result in enhanced and more long-lived revivals with increasing ξ. Importantly, the local squeezing gives significantly better results, leading to almost perfect revivals and thus supporting the physical reasoning outlined above.

Hamiltonian deformations.—Our interpretation of the PXP dynamics in terms of a scattering problem has motivated deformations of the initial states in order to enhance the periodic dynamics associated with QMBS in the PXP model. In a complementary view, one might instead deform the Hamiltonian and leave the initial state invariant. Specifically, instead of squeezing the initial state, we can in a unitarily equivalent way conjugate the Hamiltonian with the squeezing operators, appropriately symmetrized across the two partitions [28], to obtain $H_{\chi,\text{global}} = V_\chi^\dagger H V_\chi$ or $H_{\chi,\text{local}} = U_\chi^\dagger H U_\chi$, respectively. Clearly, these transformed Hamiltonians will induce enhanced revivals with increasing χ, that now occur for the plain $|\mathbb{Z}_2^A\rangle$ initial state rather than its squeezed counterpart. Thus, our analysis ultimately allows

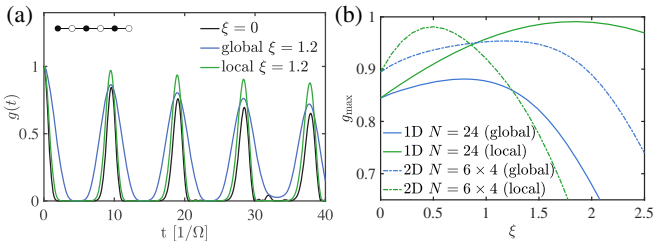

FIG. 3. (a) Many-body fidelity $g(t)$ for a 1D circle with $N = 24$, initialized in both an unsqueezed ($\xi = 0$) and globally and locally squeezed ($\xi = 1.2$) initial $\mathbb{Z}_2$ state. (b) First maximum of the many-body fidelity $g_{\max}$ as a function of squeezing parameter ξ, for initial $\mathbb{Z}_2$ states squeezed both globally and locally, on 1D and 2D lattices with $N = 24$ sites.

us to construct a deformation of the PXP Hamiltonian that gives rise to perfect revivals on the infinite CBG and significantly enhanced revivals on other lattices. For instance, in 1D the deformed Hamiltonian is

$$H_{\chi,\mathrm{local}} = H - \frac{\Omega\chi}{2}\sum_i \mathcal{P}\sigma_i^x\mathcal{P}(\sigma_{i-2}^z + \sigma_{i+2}^z) + O(\chi^2). \quad (11)$$

Remarkably, the leading order terms introduced by this deformation are of the same form as those studied in Refs. [6,7], where it was shown that they lead to virtually perfect QMBS. However, the physical motivation for the particular form of such deformations has remained uncertain. In contrast, these deformations emerge naturally in the scattering picture developed in this work. This highlights one of the main merits of the scattering approach.

Discussion.—In this work we have discussed the phenomenon of QBMS in PXP models, developing a new analytical approach to studying QMBS based on an equivalence between the PXP model on the CBG and a 1D chiral scattering problem. The resulting novel insights into the mechanism underlying scars in PXP models allow the conclusion that dynamical signatures of QMBS can be enhanced by spin squeezing. This could prove a valuable tool for quantum information processing tasks based on quantum many-body scars [39], and could potentially be combined with other approaches of actively stabilizing QMBS, for instance through driving [8,9,40,41].

While our focus on PXP models on CBGs is motivated by the analytical tractability, we note that such models could be potentially realized in Rydberg atom array experiments. For instance, in a two-species setting [42] with appropriately chosen Rydberg states, weak intraspecies interactions and strong interspecies interactions could result in an effective PXP model on the CBG where the two atomic species represent the two partitions.

We thank M. Endres, S. Choi, W. W. Ho, G. Giudici and H. Bernien for useful discussions. This work is supported by the Erwin Schrödinger Center for Quantum Science and Technology through a Discovery Grant.

Note added—After completing this work, an independent study of a related model appeared in Ref. [43].

*Hannes.Pichler@uibk.ac.at

[1] J. M. Deutsch, Phys. Rev. A **43**, 2046 (1991).
[2] M. Srednicki, Phys. Rev. E **50**, 888 (1994).
[3] M. Rigol, V. Dunjko, and M. Olshanii, Nature (London) **452**, 854 (2008).
[4] M. Serbyn, D. A. Abanin, and Z. Papic, Nat. Phys. **17**, 675 (2021).
[5] H. Bernien, S. Schwartz, A. Keesling, H. Levine, A. Omran, H. Pichler, S. Choi, A. S. Zibrov, M. Endres, M. Greiner, V. Vuletić, and M. D. Lukin, Nature (London) **551**, 579 (2017).
[6] V. Khemani, C. R. Laumann, and A. Chandran, Phys. Rev. B **99**, 161101(R) (2019).
[7] S. Choi, C. J. Turner, H. Pichler, W. W. Ho, A. A. Michailidis, Z. Papic, M. Serbyn, M. D. Lukin, and D. A. Abanin, Phys. Rev. Lett. **122**, 220603 (2019).
[8] D. Bluvstein, A. Omran, H. Levine, A. Keesling, G. Semeghini, S. Ebadi, T. T. Wang, A. A. Michailidis, N. Maskara, W. W. Ho, S. Choi, M. Serbyn, M. Greiner, V. Vuletic, and M. D. Lukin, Science **371**, 1355 (2021).
[9] A. A. Michailidis, C. J. Turner, Z. Papic, D. A. Abanin, and M. Serbyn, Phys. Rev. Research **2**, 022065(R) (2020).
[10] S. Ok, K. Choo, C. Mudry, C. Castelnovo, C. Chamon, and T. Neupert, Phys. Rev. Research **1**, 033144 (2019).
[11] D. K. Mark and O. I. Motrunich, Phys. Rev. B **102**, 075132 (2020).
[12] S. Moudgalya, B. A. Bernevig, and N. Regnault, Phys. Rev. B **102**, 195150 (2020).
[13] D. K. Mark, C.-J. Lin, and O. I. Motrunich, Phys. Rev. B **101**, 195131 (2020).
[14] K. Bull, I. Martin, and Z. Papic, Phys. Rev. Lett. **123**, 030601 (2019).
[15] C.-J. Lin and O. I. Motrunich, Phys. Rev. Lett. **122**, 173401 (2019).
[16] M. Schecter and T. Iadecola, Phys. Rev. Lett. **123**, 147201 (2019).
[17] T. Iadecola, M. Schecter, and S. Xu, Phys. Rev. B **100**, 184312 (2019).
[18] S. Chattopadhyay, H. Pichler, M. D. Lukin, and W. W. Ho, Phys. Rev. B **101**, 174308 (2020).
[19] S. Moudgalya, E. O'Brien, B. A. Bernevig, P. Fendley, and N. Regnault, Phys. Rev. B **102**, 085120 (2020).
[20] C. J. Turner, A. A. Michailidis, D. A. Abanin, M. Serbyn, and Z. Papić, Nat. Phys. **14**, 745 (2018).
[21] C. J. Turner, A. A. Michailidis, D. A. Abanin, M. Serbyn, and Z. Papic, Phys. Rev. B **98**, 155134 (2018).
[22] W. W. Ho, S. Choi, H. Pichler, and M. D. Lukin, Phys. Rev. Lett. **122**, 040603 (2019).
[23] A. A. Michailidis, C. J. Turner, Z. Papic, D. A. Abanin, and M. Serbyn, Phys. Rev. X **10**, 011055 (2020).
[24] I. Lesanovsky, Phys. Rev. Lett. **108**, 105301 (2012).
[25] D. Jaksch, J. I. Cirac, P. Zoller, S. L. Rolston, R. Cote, and M. D. Lukin, Phys. Rev. Lett. **85**, 2208 (2000).
[26] M. Saffman, T. G. Walker, and K. Molmer, Rev. Mod. Phys. **82**, 2313 (2010), publisher: APS.
[27] H. Weimer, M. Müller, I. Lesanovsky, P. Zoller, and H. P. Büchler, Nat. Phys. **6**, 382 (2010).
[28] See Supplemental Material at http://link.aps.org/supplemental/10.1103/PhysRevLett.128.090606 for a review on spin coherent states and the Holstein-Primakoff transformation as well as a derivation of the analytical expressions for the scattering coefficients and the deformed Hamiltonian, which includes Refs. [29–34].
[29] D. F. Walls and G. J. Milburn, *Quantum Optics*, 2nd ed. (Springer, New York, 2008).
[30] J. Gazeau, *Coherent States in Quantum Physics* (Wiley-VCH, New York, 2009).
[31] T. Guaita, L. Hackl, T. Shi, E. Demler, and J. I. Cirac, Phys. Rev. Research **3**, 023090 (2021).
[32] B. M. Garraway, Phil. Trans. R. Soc. A **369**, 1137 (2011).

[33] A. Klein and E. R. Marshalek, Rev. Mod. Phys. **63**, 375 (1991).
[34] M. Abramowitz and I. A. Stegun, *Handbook of Mathematical Functions*, 10th ed., Applied Mathematics Series No. 55 (National Bureau of Standards, Washington, 1972).
[35] J. M. Radcliffe, J. Phys. A: Gen. Phys. **4**, 313 (1971).
[36] J. Ma, X. Wang, C. P. Sun, and F. Nori, Phys. Rep. **509**, 89 (2011).
[37] C. Gross, J. Phys. B **45**, 103001 (2012).
[38] M. Kitagawa and M. Ueda, Phys. Rev. A **47**, 5138 (1993).
[39] S. Dooley, PRX Quantum **2**, 020330 (2021).
[40] B. Mukherjee, S. Nandy, A. Sen, D. Sen, and K. Sengupta, Phys. Rev. B **101**, 245107 (2020).
[41] S. Sugiura, T. Kuwahara, and K. Saito, Phys. Rev. Research **3**, L012010 (2021).
[42] K. Singh, S. Anand, A. Pocklington, J. T. Kemp, and H. Bernien, arXiv:2110.05515.
[43] J. Desaules, K. Bull, A. Daniel, and Z. Papic, arXiv:2112.06885.